WELDING RESEARCH

SUPPLEMENT TO THE *WELDING JOURNAL*, AUGUST 1992

Sponsored by the American Welding Society and the Welding Research Council

Fatigue Life Prediction of Cruciform Joints Failing at the Weld Toe

A two-stage model appears to offer the most accuracy in predicting fatigue life

BY M. SKORUPA

ABSTRACT. The objective of this study is to select a theoretical model to predict the fatigue life of a weld. The experimental part consists of fatigue tests within the life range of from 10^5 to 2×10^6 cycles for cruciform welded joints in two structural steels under constant amplitude axial loading with a constant positive stress ratio: the fatigue crack initiating at the weld toe. The fatigue lives were then calculated according to the two-stage approach in which both the fatigue crack initiation phase and the crack propagation phase were considered, and according to the one-stage approach which assumes that the total fatigue life is spent in crack propagation. The local strain method was applied to calculate the fatigue crack initiation life, while the fatigue crack propagation life was estimated using fracture mechanics concepts. The important feature of these analyses was that the material properties needed were estimated via hardness measurements. The fatigue lives obtained by the two-stage model fall within the 0.95 confidence limits of the experimental data and are conservative in the sense that the average ratio of the observed-to-calculated life is 1.15. The one-stage model results in life estimates an order of magnitude lower than those derived from the two-stage model. The study suggests that the two-stage model rather than the one-stage model enables accurate fatigue life predictions even for welds containing undercuts.

Introduction

Analytical procedures used for predicting fatigue behavior of notched structural members can be broadly classified as the one-stage models assuming that

$$N_f = N_p \quad (1a)$$

or

$$N_f = N_i \quad (1b)$$

and the two-stage models where

$$N_f = N_i + N_p \quad (2)$$

The approaches according to Equations 1a, 1b and 2 will be further termed as the P, I and I-P models, respectively. In Equations 1 and 2, N_f is the total fatigue of life, N_p is the crack propagation life and N_i is the crack initiation life. For small metal components, N_i is defined as the number of cycles required to develop a dominant crack of a so-called initial size (a_i), usually of the order of tenths of a mm. The meaning of N_p in Equations 1a and 2 is not the same. N_p in Equation 2 is the number of cycles spent in crack growth from a_i to final fracture while N_p in Equation 1a accounts also for the earliest phase of crack growth from a flaw or a microstructure defect. Usually, low-cycle-fatigue theory is adopted to estimate N_i, and fracture mechanics is employed to calculate N_p.

Disagreement prevails on which of the models defined by Equations 1 and 2 best reflects fatigue behavior of welds. A widespread opinion that defects, usually crack-like in shape, are unavoidable even in high-quality welds involves the predominant use of the P model (Refs. 1–3). However, successful estimates of weld fatigue life have also been made utilizing the two-stage approach (Ref. 4).

Fatigue analysis of welds requires that strength effects of the welding process be accounted for. The most important of these are: geometrical variability, change of material properties in the weld neighborhood and residual stresses.

The objective of this paper was to select the theoretical model most adequate for predicting the total fatigue life of a weld. The study focused on a cruciform welded joint in two structural steels under constant amplitude axial loading. The dimensions of the weldment were chosen such that failure occurred at the weld toe. Fatigue lives calculated according to the two-stage and one-stage models for a defectless weld geometery and in the presence of undercut were compared with the observed results.

KEY WORDS

Modeling
Fatigue Life
Cruciform Joints
Structural Steels
Weld Toe Cracking
Crack Initiation
Crack Propagation
Local Strain
Fracture Mechanics
Hardness Measure

Experimental Tests

Specimens

Cruciform welded specimens for fatigue testing were fabricated from structural steel plates. The steels were St3S (carbon mild steel) and 18G2A (low-alloy steel). The chemical compositions and mechanical properties of these steels are given in Table 1. The welding procedure was manual metal arc in the horizontal position. Based on Ref. 1, the ratios of the weld leg length l to the plate thickness t were chosen such to promote failure at the weld toe under axial fatigue loading. The St3S plates were welded in longer pieces and then saw-cut into narrow specimens. Each 18G2A specimen was welded separately. The specimen side surfaces were milled to discard weld start and stop areas, then ground. The specimen geometry is shown in Fig. 1 and the dimensions are given in Table 2.

Variable geometry parameters (Fig. 2), knowledge of which is vital to analytical fatigue life prediction, namely, the weld contact angle β, the notch root radius at the weld toe r, the depth of possible undercut at the weld toe d and misalignment (eccentricity e and angular distortion α),

M. SKORUPA is with the University of Mining and Metallurgy, Krakow, Poland.

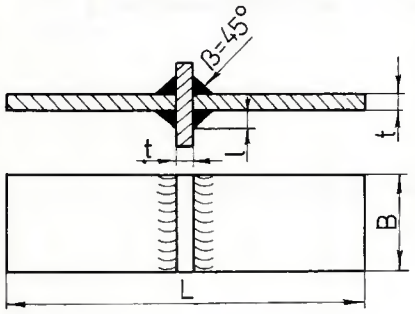

Fig. 1—Test specimen geometry.

were measured. The measurements of the β and r values were made in side surfaces of the specimens using an optical microscope at a magnification of 10×. While only small variations in the β values were observed due to very smooth weld profiles (Fig. 3A), the measured r values showed a large amount of scatter (Fig. 3B).

Undercuts were macroscopically examined at magnification of about 70× in 19 longitudinal sections of the St3S specimens and in 35 sections of the 18G2A specimens; four weld toe regions being observed in each section. Preparation of that inspection involved wet polishing with successively finer grades of emery paper. Undercut depths were measured perpendicularly to the intended direction of loading from a horizontal projection of the base plate line—Fig. 2. No undercuts except several very shallow (of depth below 0.05 mm) depressions at the weld toe were detected in the St3S specimens. However, in the 18G2A specimen sections 82 undercuts were found for the total number of 140 weld toe regions inspected. The measured depths d did not exceed 0.1 mm (Fig. 3C), the notch root radius at the bottom of undercut r′ being always larger than d.

The way of fabrication of the 18G2A specimens achieved a very good joint alignment. Misalignments, namely eccentricity up to 20% of the plate thickness and angular distortions up to 3 deg (Fig. 2) were only found in part of the St3S specimens. As a rule, the values of e and α measured in both sides of a given specimen were not the same. The maximum values of e and α for the St3S specimens are listed in Table 3.

Table 2—Dimensions of Welded Specimens

Material	Ratio l/t	Dimensions (mm) t	l	B	L
St3S	1	12	12	35	400
	1.5	10	15	35	400
18G2A	1.5	10	15	60	400

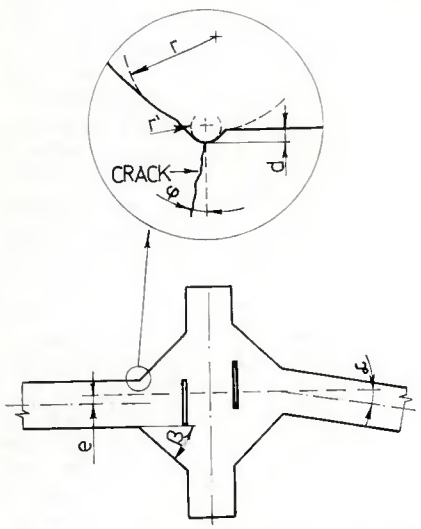

Fig. 2—Variable geometry parameters and crack path for test specimens.

Table 1—Chemical Composition and Mechanical Properties of the Steels Used for Welded Specimens

Steel	Chemical Composition (%) C	Mn	Si	P	S	Cr	Cu	Mechanical Properties S_u (MPa)	S_y (0.2%, MPa)	RA %
St3S	0.18	0.47	0.15	0.037	0.034	0.020	0.020	440	282	58
18G2A	0.11	1.78	0.54	0.026	0.020	0.020	0.040	525	359	52

Fatigue Tests

The specimens were fatigue tested until failure by breaking into two parts in an electrohydraulic machine under constant stress amplitude at a frequency of ≈15 Hz. The stress ratio R was 0.1 for the St3S specimens and 0.2 for the 18G2A specimens. All the 1/t = 1.5 specimens failed at the weld toe, while in part of the 1/t = 1 specimens weld failures were observed in accordance with other reported results (Ref. 1). Tables 3 and 4 give the fatigue test results for the specimens failing at the weld toe.

A statistical analysis of the fatigue data for the Series 1/t = 1.5 St3S specimens and 18G2A specimens was carried out according to Ref. 5 assuming the following linear relationship between the fatigue life N_f and the nominal stress range ΔS:

$$\log N_f = A + B \log \Delta S \qquad (3)$$

The small number of Series l/t = 1 St3S specimens failing at the weld toe prohibited performing a statistical analysis of the corresponding fatigue data.

The fatigue test results together with the relevant regression lines and 0.95 confidence limits are shown in Figs. 4 and 5. The higher width of the scatter band for the St3S welds (Fig. 4) compared to that for the 18G2A welds (Fig. 5) may predominantly result from the occurrence of misalignments in the former specimens. The reason fatigue resistance of the St3S specimens is significantly higher than that of the 18G2A specimens may be attributed to

Table 3—Fatigue Test Results and Misalignments for St3S Specimens

Material	Ratio l/t	Nominal Stress Range ΔS (MPa)	Total Fatigue Life N_f (cycles)	Misalignments Eccentricity e (mm)	Misalignments Angular Distortion α^0
St3S	1	298.5	78 160	1.5	1
		248.3	160 000	2.0	3
			245 500	1.5	1
		195.0	907 800	0	2
			1 224 500	1.5	1
			1 349 000	1.0	0
	1.5	252.0	146 000	1.0	0
			254 000	0	2
			260 000	1.5	1
		288.5	309 000	0	1
		264.3	201 500	1.0	3
			246 000	2.0	0
			282 000	2.0	0
			630 000	1.0	1
		236.4	476 000	1.0	0
			671 000	2.0	2
			844 000	1.0	2
			988 000	0	0
		205	1 005 000	2.0	0
			1 367 000	1.0	1
			1 666 000	1.5	2
			Unbroken	0	0

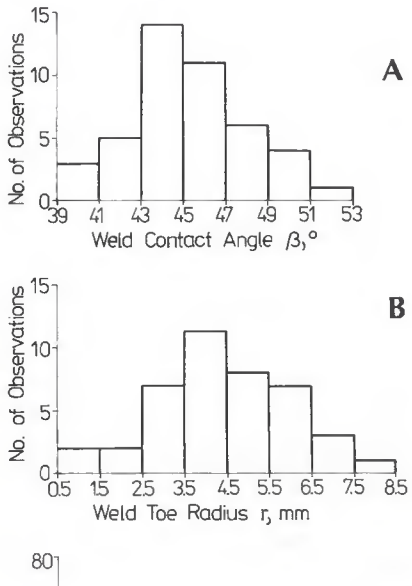

Fig. 3—Measured variations of geometry parameters for test specimens: A—Weld contact angle β, B—Root radius at the weld toe r; C—Depth of undercut d.

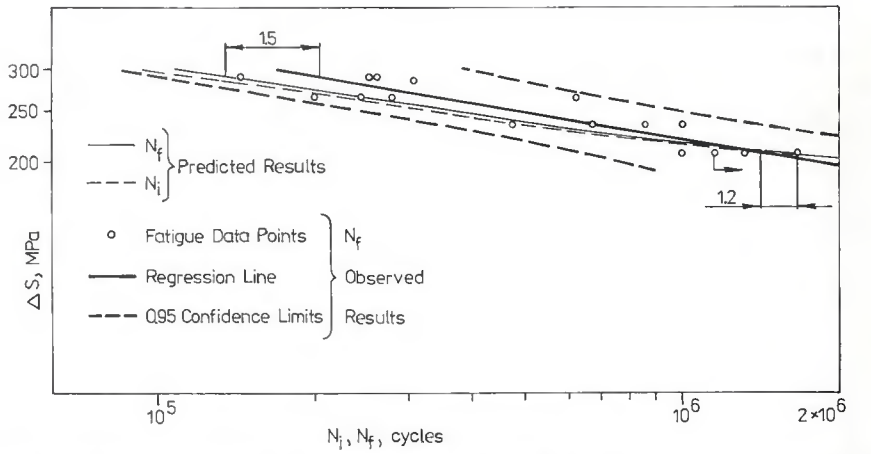

Fig. 4—Observed and predicted with two-stage approach fatigue lives for St3S l/t = 1.5 welded specimens.

more favorable weld toe geometry (lack of undercuts) in the former. The present fatigue data fall within the reported scatter bands obtained with similar specimens (Ref. 1).

Microscopic examination of the cracked specimens revealed that fatigue cracks initiated and propagated within the heat-affected zone (HAZ). Fatigue crack paths were approximately straight lines sloped to the direction transverse to the main plate at an angle $\phi \approx 15$ deg for l/t = 1.5 and $\phi \approx 8$ deg for l/t = 1 (Fig. 2). An observation of the fracture surfaces indicated that the specimens failed when the crack depth reached on an average about 0.35t.

Fatigue Life Calculations

Geometrical Variability

Based on the geometry measurements (Fig. 3), the variations in the angle β are ignored and an average value of $\beta = 45$ deg is assumed. In order to cope with the variable nature of other geometry parameters at the weld toe, it is assumed, after Lawrence, *et al.* (Ref. 4), that fatigue cracking starts at the location where the fatigue notch factor calculated through Peterson's equation adopts its maximum value.

Peterson's equation reads

$$K_f = 1 + \frac{K_t - 1}{1 + \alpha/r} \qquad (4)$$

where K_t is the elastic stress concentration factor, r is the notch root radius and α is a material constant given by $2.32 \times 10^4 S_u^{-1.8}$ (mm), S_u being the ultimate strength of material in MPa.

If the analytical K_t vs. r relationship is known, Equation 4 can be differentiated with respect to r to determine the critical notch root radius r_c for which K_f obtains a maximum.

For the defectless weld toe geometry, the following K_t vs. r relationship was obtained from finite element analysis (Ref. 6):

$$K_t = 1 + C_1(r/t)^{C_2} \qquad (5)$$

where the constants C_1 and C_2 depend on the ratio of 1/t.

The K_f function given by Equation 4 combined with Equation 5 passes through a maximum for

$$r_c = \frac{C_2 + 1}{C_2} - a \qquad (6)$$

In the presence of undercut (Fig. 2) the theoretical stress concentration factor at the weld toe was approximated by (Ref. 7)

$$K_{tu} = K_t\left(1 + 2\sqrt{(d/r')}\right) \qquad (7)$$

where K_t is given through Equation 5.

Using Equations 4 and 7, the fatigue

Table 4—Fatigue Test Results for 18G2A Specimens

Material	Ratio l/t	Nominal Stress Range ΔS (MPa)	Total Fatigue Life N_{f1} (cycles)
18G2A	1.5	223	135 000
			180 000
		200	159 600
		175	363 700
		171	236 100
		168	324 900
			346 300
			371 500
		140	524 100
			821 300
			861 600
		119	1 159 900
			1 291 100
			Unbroken

Table 5—Empirical Relationships between Mechanical Properties and Hardness DPH of Steel

Property	Function of DPH	Sources
Ultimate tensile strength, S_u (MPa)	3.45 DPH	Ref. 8
Yield strength 0.2%, S_y (MPa)	2.68 DPH − 138	Ref. 9
Fatigue strength coefficient, σ_f' (MPa)	3.3 DPH + 370	Ref. 9
Fatigue strength exponent, b	$-\frac{1}{6}\log(2.1 + 266/\text{DPH})$	Ref. 9
Cyclic yield strength, σ_y' (MPa)	2.1 DPH	Ref. 8
Transition fatigue life, $2N_{tr}$ (reversals)	$5.7 \times 10^S \exp(-0.017\ \text{DPH})$	Ref. 9

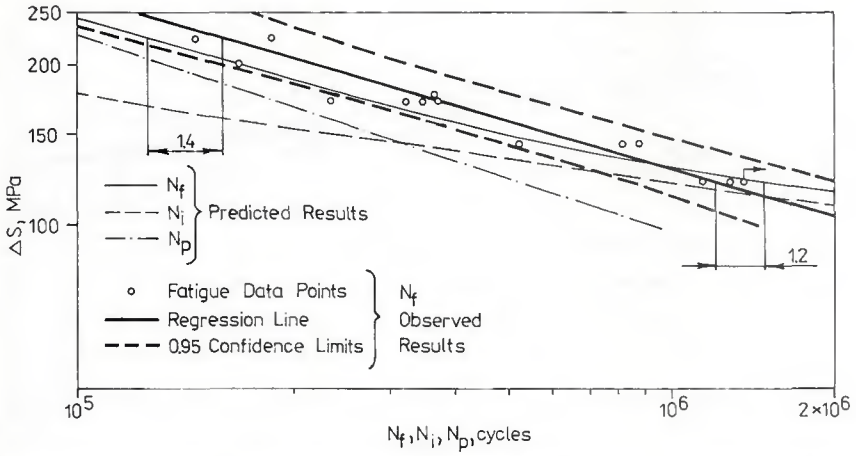

Fig. 5—Observed and predicted with two-stage approach fatigue lives for 18G2A welded specimens.

notch factor for a weld with undercut was obtained as

$$K_f = 1 + \frac{K_t\,(1 + \sqrt{(d/r')}) - 1}{1 + a/r'} \qquad (8)$$

From Equation 8, the K_{fmax} condition for a weld with undercut exists if

$$r' = \left[\frac{\sqrt{(a^2\,(K_t - 1)^2 + 4K_t^2}}{2\,K_t\,a\,\sqrt{d}}\right]^{-2} \qquad (9)$$

Based on the inspection of the weld toe regions described earlier, the St3S specimens were assumed to be defectless while for the 18G2A specimens the presence of undercuts was allowed for. According to the K_{fmax} concept, Equations 6 and 9 define the values of the notch root radius adopted in the crack initiation and crack propagation analyses for the St3S and 18G2A specimens, respectively. As the fatigue notch factor according to Equation 8 is a monotonic function of r and d, the minimum measured r value equal to 0.5 mm and the maximum measured d value equal to 0.1 mm were assumed for the 18G2A specimens.

Estimating HAZ Material Properties through Hardness Measurements

The properties of the HAZ material that are involved in the fatigue process of the test specimens may be different from those of the base metal. As HAZ material is difficult and expensive to test, all the required material parameters were either estimated from hardness measurements at the weld toe using empirical relationships given in Table 5 or assumed.

The fatigue ductility exponent c = −0.6 was assumed. The relationships of S_y and σ_y' with hardness depend on the type of steel. As discussed in Ref. 7, those assumed in Table 5 correlate best with reported test results for various HAZ materials in steels (Refs. 4, 9).

Other material properties of the HAZ were calculated through the following relationships that are known in the low-cycle-fatigue theory:

cyclic strain hardening exponent

$$n' = b/c \qquad (10)$$

cyclic strength coefficient

$$K' = \sigma_y'/(0.002)^{n'} \qquad (11)$$

fatigue ductility coefficient as the mean of

$$\epsilon_f' = (\sigma_f'/K')^{1/n'} \qquad (12)$$

and

$$\epsilon_f' = \sigma_f'(2N_{tr})^{b-c}/E \qquad (13)$$

Table 6 lists the material properties calculated from the relationships given in Table 5 and from Equations 10 to 13. The values of r_c, r_c' and K_{fmax} in Table 6 result from Equations 4 to 9.

Initial and Final Crack Size

Where the I-P model (Equation 2) is employed, the initial crack size a_i must be defined in order to bridge between the initiation and propagation analyses. A common practice is to assume the a_i value arbitrarily (usually 0.25 mm), although nonarbitrary definitions of a_i were also proposed (Refs. 10, 11). For the considered geometry and material it was shown in Ref. 7 that the value of 0.25 mm lies between those calculated according to Refs. 10 and 11. Therefore, a_i = 0.25 mm was adopted in this study. Based on the examination of fracture surfaces, the final crack size a_f = 3.5 mm was assumed.

Residual Stresses

The way of fabrication of both St3S and 18G2A specimens precluded occurrence of high residual stresses. With the narrow 18G2A specimens, making a weld produced a more or less even temperature across the plates and consequently could only create low residual stresses. Although relatively high residual stresses were likely to occur in the St3S welds before cutting up the plates, they were relieved by the slicing operation (Ref. 1). Therefore, residual stresses were ignored in the present analysis.

Residual stresses when present can be allowed for in the crack initiation analysis as a static prestress (Refs. 12 and 13).

Crack Initiation Analysis

The crack initiation lives (N_i) were estimated with the local strain approach (Ref. 14). The mathematical procedure to calculate the local stress and strain amplitudes (σ_α and ϵ_α, respectively) and the local mean stress (σ_o) is illustrated in Fig. 6 where R is the stress ratio, S and e denote the nominal stress and strain, respectively, and the subscripts "1" and "a" to stress or strain correspond to the value at the end of the first loading reversal and to the amplitude, respectively. Since the material properties involved in the monotonic stress-strain curve equation cannot be related to hardness, cyclic softening of HAZ material was ignored.

The N_i values were calculated through the equation from Morrow (Ref. 15)

$$\sigma_\alpha = (\sigma_f' - \sigma_o)(2N_i)^b \qquad (14)$$

in which only the material properties that can be directly related to hardness are utilized.

To allow for the effect of cyclic relaxation of the local mean stress on N_i the constant σ_o value in Equation 14 was replaced by (Ref. 16)

$$\sigma_{o,2N} = \sigma_o\,(2N\text{-}1)^k \qquad (15)$$

where $\sigma_{o,2n}$ is the current value of mean stress at any reversal 2N and k denotes the relaxation exponent.

From Ref. 12, k was expressed through the following empirical relationship valid for metals:

$$k = -31912.5\epsilon_{p\alpha}/(E\epsilon_{tr}) \qquad (16)$$

where $\epsilon_{p\alpha}$ is the plastic strain amplitude, ϵ_{tr}: the transition strain (half strain amplitude corresponding to the transition fatigue life $2N_{tr}$), and E: the Young modulus in MPa.

The operational details and the programming flow diagrams of the procedure used to compute N_i can be found elsewhere (Ref. 7).

Crack Propagation Analysis

Since the material constants associated with fatigue crack propagation rate cannot be estimated from hardness, only the concepts where crack growth rate is described in terms of low-cycle-fatigue material properties were used in the crack propagation analysis, namely the LEFM model from Majumdar and Morrow (Ref. 17) and the EPFM approach of Usami (Ref. 18). Both above mentioned concepts were shown in Ref. 7 to provide for a welded joint in mild steel the N_p values, which correlated well with those obtained using the Paris equation.

According to the model of Majumdar and Morrow (Ref. 17) the material ahead of the crack tip within the reversed plastic zone is composed of the uniaxial "fatigue elements" of a width of $2\rho^*$ where ρ^* is a "microstructure size." Assuming that fatigue crack extension occurs due to the successive fatigue failure of each element Majumdar and Morrow deduce the following expression for fatigue crack growth rate:

$$\frac{da}{dN} = -\frac{2(b+c)}{b+c+1}\left[\frac{\sigma_y'}{4(1+n')\sigma_f'\epsilon_f'}\right]^{\frac{-1}{b+c}} \left\{\left(1+\frac{\rho^*\pi\sigma_y'^2}{\epsilon_y'\Delta K^2}\right)^{\frac{b+c+1}{b+c}} + -[4(1+n')\epsilon_y']^{-\frac{b+c+1}{b+c}}\right\}\frac{\epsilon_y\Delta K^2}{\pi\sigma_y^2} \quad (17)$$

where ΔK is the stress intensity factor range, ϵ_y' is the cyclic yield strain, and the meaning of the other symbols is explained in Table 6.

The validity of Equation 17 is limited by the condition

$$R_p >> 2\rho^* \quad (18)$$

where R_p is the reversed plastic zone size.

The physical interpretation of ρ^* given by Majumdar and Morrow (Ref. 17) suggests that it represents the mean distance between the major microstructure deformation barriers. This distance is thought to be closely related to the length of a nonpropagating surface crack at the fatigue limit (Ref. 19). According to Usami (Ref. 18), the diameter (d_{pc}) of such a crack in a metallic material is a material constant which can be expressed as

$$d_{pc} = 1.633 \times 10^{-7}(S_y/E)^{-2}\ (mm) \quad (19)$$

The above mentioned findings from Refs. 18 and 19 are the rationale for assuming in the present analysis that ρ^* equals d_{pc}.

Equation 17 was only utilized to calculate the crack propagation lives for the St3S specimens. The approach of Usami (Ref. 18) was applied to derive the N_p estimates for the 18G2A specimens since Equation 18 was not satisfied for 18G2A HAZ material even at the highest stress level considered. From experimental tests on various steels, Usami postulates a correlation between the normalized crack growth rate $(da/dn)/a_e$, a_e being the effective crack length (half length of a central crack in an infinite body) and the effective local strain range given by

$$\Delta\epsilon_{eff} = \Delta\epsilon/(1\text{-}R), \quad R \leq O$$
$$\Delta\epsilon_{eff} = \Delta\epsilon, \quad R > O \quad (20)$$

where $\Delta\epsilon$ and R are the total local strain range and the local stress ratio, respectively, at a distance of a from the notch root in the uncracked body.

Usami's experimental data points can be fitted in with the following relationships:

Table 6—Mechanical Properties of St3S HAZ and 18G2A HAZ Material

Property	St3S HAZ	18G2A HAZ
Hardness, DPH	170	153
Ultimate strength, S_u (MPa)	587	528
Yield strength 0.2%, S_y (MPa)	318	272
Young modulus, E (MPa)	200000	200000
Cyclic yield strength, α_y'(MPa)	357	321
Fatigue strength coefficient, σ_f'(MPa)	930	875
Fatigue strength exponent, b	−0.094	−0.097
Fatigue ductility coefficient, ϵ_f'	0.878	0.937
Fatigue ductility exponent, c	−0.6	−0.6
Cyclic hardening exponent, n'	0.157	0.162
Cyclic strength coefficient, K'(MPa)	947	878
Transition fatigue life, $2N_{tr}$ (reversals)	31678	42294
Peterson's material constant, α (mm)	0.242	0.292
Critical notch root radius, r_c [r_c'] (mm)	0.167[a] 0.157[b]	[0.74]
Maximum fatigue notch factor, K_{fmax}	1.995[a] 2.93[b]	3.12

(a) l/t = 1.5
(b) l/t = 1

$$(da/dN)/a_e = 12.3(\Delta\epsilon_{eff})^2 \quad \Delta\epsilon_{eff} \leq 9 \times 10^{-4}$$
$$(da/dN)/a_e = 64800(\Delta\epsilon_{eff})^{9.22} \quad 9 \times 10^{-4} < \Delta\epsilon_{eff} < 5 \times 10^{-3}$$
$$(da/dN)/a_e = 101(\Delta\epsilon_{eff})^2 \quad \Delta\epsilon_{eff} \geq 5 \times 10^{-3} \quad (21)$$

From Ref. 18, Equation 21 proved valid for a number of steels.

In order to calculate the N_p values Equations 17 and 21 were integrated numerically in 24 steps employing Simpson's rule. The stress intensity factor solution was derived by finite element method, as described thoroughly in Ref. 6.

Comparison of Predicted and Observed Results

Two-Stage Approach

In Figs. 4 and 5 the total fatigue lives N_f provided via the two-stage I-P model (Equation 2) are compared with the fa-

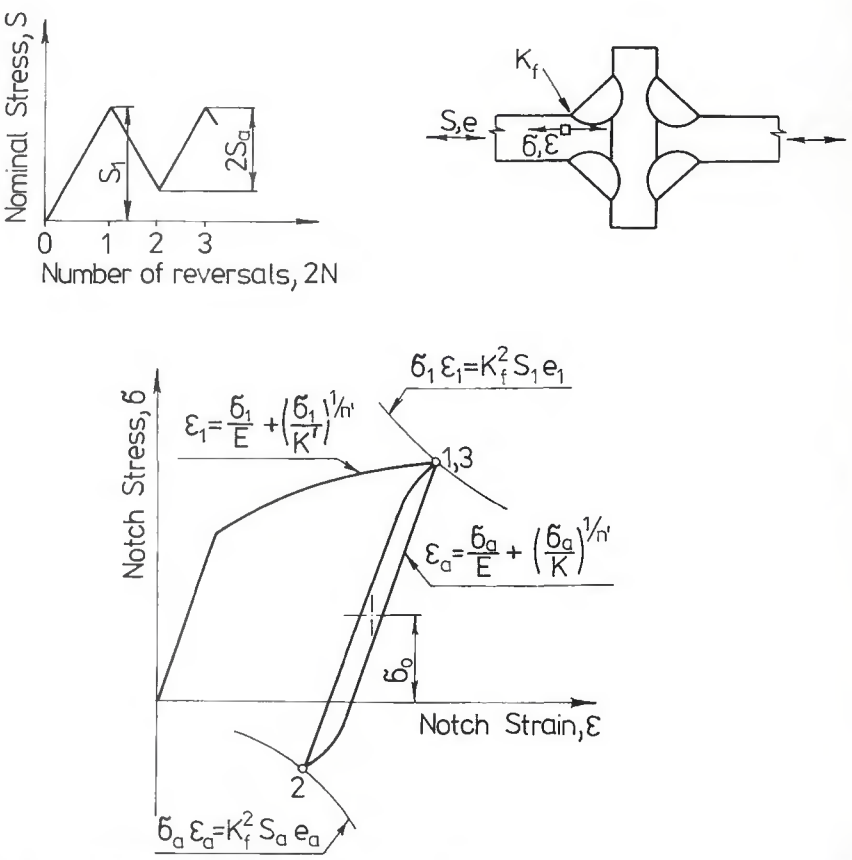

Fig. 6—Schematic of notch stress and strain calculation.

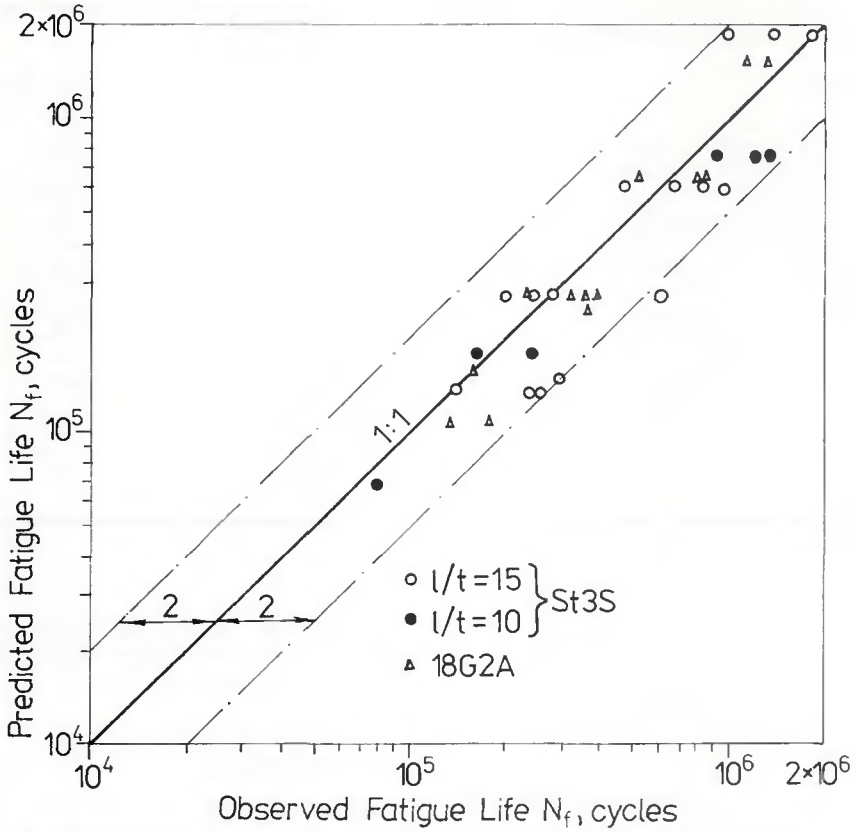

Fig. 7—Comparison between observed and predicted fatigue lives for all test specimens.

tigue test data for the welded specimens. The discrepancies between the predicted ΔS vs. N_f diagrams and the regression lines are depicted by ratios of N_f values given for the two stress levels that correspond to the highest and the lowest stress range considered in the experimental tests. From Figs. 4 and 5, it is seen that the predicted ΔS vs. N_f curves fall within the scatter bands of the fatigue data. Since the slopes of the theoretical ΔS vs. N_f diagrams in Figs. 4 and 5 are lower than these of the regression lines, the mean fatigue lives (represented by the regression lines) are underestimated at higher stress levels and slightly overestimated at lower stress levels.

The comparison between the actual and calculated fatigue lives for all the fatigue specimens is given in Fig. 7. Except

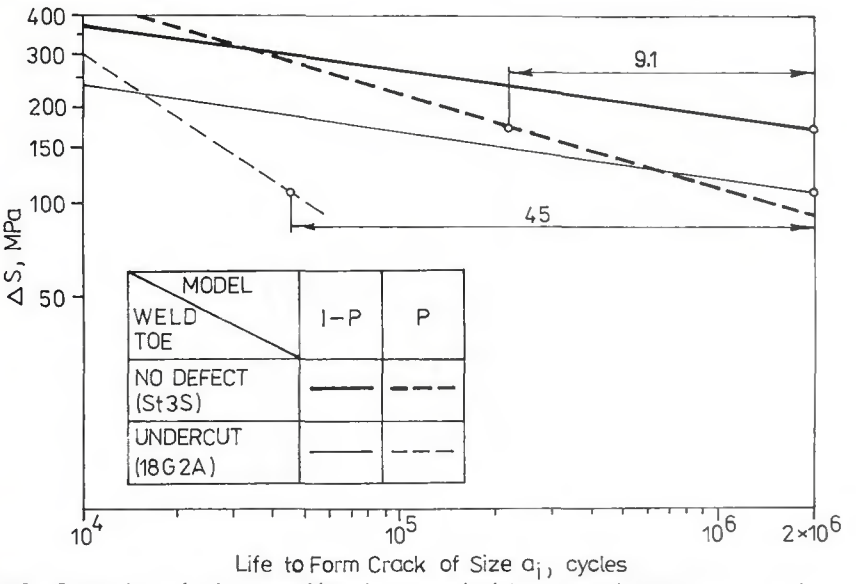

Fig. 9—Comparison of estimates on life to form a crack of size a_i according to two-stage and one-stage model for sound weld and for weld with undercut.

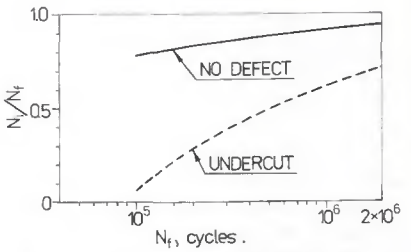

Fig. 8—Predicted percentage of total life devoted to fatigue crack initiation as a function of total life for sound weld and for weld with undercut.

a single data point, the predictions agree with the experimental results within a factor of 2. The predictions are conservative in the sense that the average ratio of the observed-to-calculated life is 1.15. Generally lower discrepancies between the actual and estimated results observed in Fig. 7 for the 18G2A specimens compared to those for the St3S specimens are aparently due to the higher scatter in the fatigue data in the latter case.

In Fig. 8 the predicted percentage of total life spent in crack initiation is plotted as a function of total life. For a sound weld, the figure shows that within the considered life range crack initiation consumes a prevailing fraction of life while in the presence of undercut, crack initiation life dominates only in the long life regime ($N_f > 5 \times 10^5$ cycles).

One-Stage Approach

As discussed previously, the difference between life estimates according to the two-stage and the one-stage (P model) approaches arises from the different ways of predicting the number of cycles to develop a crack of size a_i.

In Fig. 9 the evaluations of that number of cycles for the considered cruciform weld by using the I-P model and the P model are compared, Usami's concept (Ref. 18, see Equations 20 and 21) being employed in the latter case. It can be seen in Fig. 9 that the P model gives more conservative predictions on the life to form a crack of size a_i than the I-P model. The discrepancies between that life estimate from both approaches increase with decreasing stress level to reach the value of 9.1 for the sound weld and 45 for the weld with undercut. Considering that the I-P model has been previously shown to yield slightly conservative N_i estimates (Figs. 4, 5 and 7), from Fig. 9, it is clear that for lives greater than 10^5 cycles the P model cannot entirely account for the total fatigue life even for a weld containing undercut.

Final Remarks

Although based on the material properties estimated in a rough way, the fatigue lives predicted using the two-stage

approach are in good agreement with the experimental results. Utilizing in fatigue analyses of welds the HAZ material properties estimated via hardness measurements at the weld toe was first proposed by Lawrence, *et al.* (Ref. 4). The subsequent analyses, however, were confined to the predictions of the long life fatigue strength of welds with the use of the one-stage I model (Ref. 20). This study including the crack propagation period estimated according to the concepts in which the fatigue crack growth rate is expressed in terms of the low-cycle-fatigue material properties, enabled life predictions within the range of from 10^5 to 2×10^6 cycles.

Conclusions

The two-stage approach, including both the fatigue crack initiation and propagation phases, enables one to estimate total fatigue lives in the life regime of 10^5 to 2×10^6 cycles, which agree within a factor of 2 with experimental data for cruciform welded specimens failing at the weld toe.

The study supports the applicability of heat-affected zone material properties estimated via hardness measurements towards fatigue life predictions of welds.

The one-stage approach, which neglects the fatigue crack initiation phase, cannot entirely account for the total fatigue life, even for welds containing undercuts.

References

1. Gurney, T. R. 1979. *Fatigue of Welded Structures.* Cambridge, U.K.

2. Yamada, K., and Hirt, M.A. 1982. Fatigue crack propagation from fillet weld toe. *J. of the Structural Division.* ASCE 108, No. ST7, pp. 1526–1539.

3. Smith, I.F.C., and Smith, R.A. 1983. Fatigue crack growth in a fillet welded joint. *Eng. Fract. Mech.* 18: 861–869.

4. Lawrence, F.V., Ho, N.J., and Mazumdar, P.K. 1981. Predicting the fatigue resistance of welds. *Annual Review of Materials Science* 8:402–425.

5. Statistical analysis of linear or linearized stress-life and strain-life fatigue data. 1980. ASTM Standard E739-80.

6. Skorupa, M., Braam, H., and Prij, J. 1987. Applicability of approximate K_I solutions towards cracks at weld toes. *Eng. Fract. Mech.* 26: 669–681.

7. Skorupa, M. 1989. Predicting the fatigue life of welds. *Scientific Bulletins of the Stanislaw Staszic Academy of Mining and Metallurgy.* No. 1257. Mechanics, Bull. 18 (in Polish).

8. Morrow, J. 1965. *Internal Friction, Damping and Cyclic Plasticity.* ASTM STP 378, pp. 45–87.

9. McMahon, J.C., and Lawrence, F.V. 1984. Predicting fatigue properties through hardness measurements. FCP Report No. 105, University of Illinois at Urbana-Champaign.

10. Chen, W. 1980. A model for joining crack initiation and propagation analyses. Ph.D. Thesis, University of Illinois at Urbana-Champaign.

11. Cameron, A.D., and Smith, R.A. 1982. Fatigue life prediction for notched members. *Int. J. of Pressure Vessels and Piping* 10: 205–217.

12. Burk, J.D. 1978. The effect of residual stresses on weld fatigue life. Ph.D. Thesis, University of Illinois at Urbana-Champaign.

13. Skorupa, M. 1990. Fatigue crack initiation life prediction for welded joints by low cycle fatigue approach. *Fat. Fract. Eng. Mater. Struct.* 13: 597–613.

14. Dowling, N.E., Brose, W.R., and Wilson, W.K. 1977. Fatigue Under Complex Loading—Analysis and Experiments. *Advances in Engineering.* SAE 6: 55–84.

15. Morrow, J. 1968. *SAE Fatigue Design Handbook,* pp. 21–30.

16. Jhansale, H.R. and Topper, T.H. 1973. Cyclic Stress-Strain Behavior. *Analysis, Experimentation, and Failure Prediction.* ASTM STP 519, pp. 246–270.

17. Majumdar, S., and Morrow, J. 1974. *Fracture Toughness and Slow Stable Cracking.* ASTM STP 559, pp. 159–182.

18. Usami, S. 1986. *Small Fatigue Cracks.* The Metallurgical Society Inc., pp. 559–585.

19. Miller, K.J. 1987. The behavior of short fatigue cracks and their initiation. *Fat. Fract. Eng. Mater. Struct.* 10: 75–91 and 93–113.

20. Yung, J.Y., and Lawrence, F.V. 1985. Analytical and graphical aids for the fatigue design of weldments. *Fat. Fract. Eng. Mater. Struct.* 8:223–241.

21. Testin, R.A., Yung, J.-Y., Lawrence, F.V., and Rice, R.C. 1987. Predicting the fatigue resistance of steel weldments. *Welding Journal* 66: 93-s to 98-s.

Appendix

a	Crack size
a_e	Equivalent crack size
a_f	Final crack size
a_i	Initial crack size
α	Peterson's material constant
b	Fatigue strength exponent
c	Fatigue ductility exponent
d	Depth of undercut
d_{pc}	Diameter of nonpropagating surface crack
e	Nominal strain
E	Modulus of elasticity
k	Relexation exponent
K_I	Stress intensity factor
K_f (K_{fmax})	Fatigue notch factor (maximum value)
K_I (K_{tu})	Stress concentration factor (at the bottom of undercut)
K'	Cyclic strength coefficient
l	Weld leg length
n'	Cyclic hardening exponent
N	Number of cycles
N_f	Total fatigue life
N_i	Crack initiation life
N_p	Crack propagation life
N_{tr}	Transition fatigue life
r (r_c)	Weld toe radius (critical value)
r' (r_c')	Root radius at the bottom of undercut (critical value)
R	Stress ratio
R_p	Reversed plastic zone size
S	Nominal stress
S_u	Ultimate tensile strength
S_y	Yield strength 0.2%
α	Angular distortion
β	Weld contact angle
ϵ	Notch strain
ϵ_p	Cyclic plastic notch strain
ϵ_{tr}	Transition strain
ϵ_f'	Fatigue ductility coefficient
ϵ_y'	Cyclic yield strain
ρ^*	Microstructure size from Majumdar and Morrow equation
σ	Notch stress
σ_o	Notch mean stress
σ_f'	Fatigue strength coefficient
σ_y'	Cyclic yield strength
ϕ	Slope of crack path

Subscripts

α	Amplitude
1	The first reversal
Δ	Range

Abbreviations

EPFM	Elastic-plastic fracture mechanics
HAZ	Heat-affected zone
LEFM	Linear-elastic fracture mechanics

Nitrogen in Arc Welding — A Review

WRC Bulletin 369
December 1991

By IIW Commission II

In 1983, Commission II of the International Institute of Welding (IIW) initiated an effort to review and examine the role of nitrogen in steel weld metals. The objective was to compile in one source, for future reference, the available information on how nitrogen enters weld metals produced by various arc welding processes, what forms it takes in these welds, and how it affects weld metal properties.

This bulletin contains 13 reports and several hundred references related to Nitrogen in Weld Metals that has been prepared as a review to show the importance nitrogen has in determining weld metal properties.

Publication of this report was sponsored by the Welding Research Council, Inc. The price of WRC Bulletin 369 is $85.00 per copy, plus $5.00 for U.S. and $10.00 for overseas, postage and handling. Orders should be sent with payment to the Welding Research Council, Room 1301, 345 E. 47th St., New York, NY 10017.

Research on Modern High-Strength Low-Alloy Steel Welding

WRC Bulletin 373
June 1992

(1) Influences of Steel Composition and Welding Procedure on the HAZ Toughness of Thick-Section Structural Steels

By P.L. Harrison and P. H. M. Hart

(2) Heat-Affected Zone Properties of Thick-Section Microalloyed Steels — A Perspective

By F. Heisterkamp, K. Hulka and A. D. Batte

(3) Experience in Fabricating New Types of Offshore Plate and Linepipe

By P. Tuvnes and I. Harneshaug

(4) Influence of Local Brittle Zone on HAZ Toughness of TMCP Steels

By S. Aihara and K. Okamoto

The four papers contained in this Bulletin were presented at the Conference on "Metallurgy, Welding and Qualification of Microalloyed (HSLA) Steel Weldments," held at Houston, Tex., November 6–8, 1990. The American Welding Society holds the copyrights and is the source of these papers. Publication of this document was sponsored by the Welding Research Council, Inc. The price of WRC Bulletin 373 is $40.00 per copy, plus $5.00 for U.S. and $10.00 for overseas, postage and handling. Orders should be sent with payment to the Welding Research Council, Room 1301, 345 E. 47th St., New York, NY 10017.